Large-energy single hits at JUNO from atmospheric neutrinos and dark matter

Bhavesh Chauhan,[*] Basudeb Dasgupta,[†] and Amol Dighe[‡]
Tata Institute of Fundamental Research, Homi Bhabha Road, Mumbai 400005, India

(Received 5 January 2022; accepted 12 April 2022; published 25 May 2022)

Large liquid scintillator detectors, such as JUNO, present a new opportunity to study neutral current events from the low-energy end of the atmospheric neutrinos, and possible new physics signals due to light dark matter. We carefully study the possibility of detecting "large-energy singles" (LES), i.e., events with visible scintillation energy > 15 MeV, but no other associated tags. For an effective exposure of 20 kton $-$ yr and considering only Standard Model physics, we expect the LES sample to contain $\sim$40 events from scattering on free protons and $\sim$108 events from interaction with carbon, from neutral-current interactions of atmospheric neutrinos. Backgrounds, largely due to β decays of cosmogenic isotopes, are shown to be significant only below 15 MeV visible energy. The LES sample at JUNO can competitively probe a variety of new physics scenarios, such as boosted dark matter and annihilation of galactic dark matter to sterile neutrinos.

DOI: 10.1103/PhysRevD.105.095035

I. INTRODUCTION

Atmospheric neutrinos are produced in the interactions of cosmic rays with Earth's atmosphere. Measurements of these atmospheric neutrinos at detectors such as Super-Kamiokande have been crucial for the discovery of neutrino oscillations [1]. Despite extraordinary achievements over several decades, the detection of low-energy nonelectron neutrino flavors, i.e., ν_μ, $\bar{\nu}_\mu$, ν_τ, and $\bar{\nu}_\tau$, has remained elusive essentially because at Cherenkov detectors like Super-Kamiokande, such a detection depends on having a charged particle above the Cherenkov threshold [2].

Scintillator detectors do not require charged particles to cross the Cherenkov threshold for them to be detected. In particular, neutral-current interactions such as $\nu + p \to \nu + p$ lead to a prompt visible scintillation, which can be detected even for neutrinos with energies of tens of MeV [3]. The difficulty is that the signal has a single component, as opposed to inverse beta decays where a neutron tag is possible in addition to the initial prompt scintillation from the charged lepton. The "singles" from neutrino sources can be mimicked by other processes, and therefore the backgrounds are usually quite large. Indeed, for small detectors, the singles from atmospheric neutrinos are often considered as a background [4,5]. However, upcoming large volume liquid scintillator detectors, such as JUNO (Jiangmen Underground Neutrino Observatory) [6], will accumulate a significant number of such singles, which may allow a first measurement of the low-energy end of the ν_μ, $\bar{\nu}_\mu$, ν_τ, and $\bar{\nu}_\tau$ atmospheric neutrino spectra.

One may ask what sources and interaction channels could lead to such singles. In a scintillator detector, the events below a few MeV visible energy will be dominated by intrinsic radioactivity. Between 5–15 MeV, the events are dominated by decays of cosmogenic isotopes. At "large" visible energies, i.e., above 15 MeV, the events are dominated by neutral-current interactions of atmospheric neutrinos. We propose that JUNO maintain a large-energy singles (LES) database comprising of singles with visible energy $E_{\rm vis} \in (15, 100)$ MeV, which will contain evidence of neutral-current interactions of atmospheric neutrinos, and possibly even of interesting physics beyond the standard model.

In this paper, we predict the LES spectrum at JUNO. We identify the main contributions to the signal in Sec. II, study the dominant backgrounds at low energy and estimate the threshold from a veto analysis in Sec. III, and present our main result in Sec. IV. Further in Sec. V, we explore well-motivated new physics scenarios that can have a visible imprint in the JUNO LES data. For example, we discuss the sensitivity to boosted dark matter and annihilation of galactic dark matter to sterile neutrinos. We end the paper with a brief summary and outlook in Sec. VI.

[*]bhavesh@theory.tifr.res.in
[†]bdasgupta@theory.tifr.res.in
[‡]amol@theory.tifr.res.in

II. SINGLES AT JUNO

The LES events from atmospheric neutrinos arise mostly from elastic scattering with protons (νp ES), and quasielasticlike scattering with carbon (νC QEL), which results in single or multiple proton knockouts. The scintillation signal from elastic scattering and "proton-only" knockouts cannot be distinguished, and the detector only measures the sum of these two channels.

The neutral-current interactions of neutrinos are sensitive to all flavors; however, they do not distinguish between flavors. Therefore, the only measurable quantity is the spectrum of the sum of events from all flavors. In general, the differential event rate with respect to the recoil energy of the proton (T_p) is given by

$$\frac{dN}{dT_p} = N_t T \sum_f \int dE_\nu \frac{d\phi^f}{dE_\nu}\frac{d\sigma^f}{dT_p}, \tag{1}$$

where $f \in \{\nu_e, \bar{\nu}_e \nu_\mu, \bar{\nu}_\mu, \nu_\tau, \bar{\nu}_\tau\}$, N_t is the number of targets, and T is the data-taking time period that we have considered to be 1 yr, unless specified. For a 20 kton fiducial volume detector, the number of target protons from hydrogen (i.e., free protons) is $N_p = 1.5 \times 10^{33}$, and the number of target carbon nuclei is $N_C = 8.8 \times 10^{32}$ [6].

A. Atmospheric neutrino fluxes

The flux of atmospheric neutrinos for $E_\nu > 100$ MeV at the site of JUNO is calculated in Ref. [7] based on the predictions of Honda *et al.* [8]. As it is located at a lower latitude than Super-Kamiokande, it is estimated that the atmospheric neutrino flux at JUNO is ∼10% smaller [7].

The atmospheric neutrino flux for $E_\nu < 100$ MeV has been determined by the FLUKA group for Super-Kamiokande and Borexino [9]. There are large uncertainties (∼25%) in the flux prediction originating from the dependence on the geomagnetic field. The predicted flux for $E_\nu < 100$ MeV at JUNO can be approximately obtained by scaling the Super-Kamiokande prediction by a factor of 0.9.

For our analysis, we use the scaled Honda *et al.* fluxes above 100 MeV and scaled FLUKA fluxes below 100 MeV with appropriate matching. Our simplified estimates agree with the predictions in Ref. [7].

B. Singles from νp ES

1. νp ES cross section

The νp ES cross section is a robust prediction of the Standard Model and has been measured experimentally [10]. The differential cross section for this process in terms of the neutrino energy (E_ν) and recoiling proton kinetic energy (T_p) is given as

$$\frac{d\sigma}{dT_p} = \frac{G_F^2 M_p^3}{4\pi E_\nu^2}\left[A \pm B\frac{s-u}{M_p^2} + C\frac{(s-u)^2}{M_p^4}\right], \tag{2}$$

where M_p is the mass of proton, $s-u = 4M_pE_\nu - 2M_pT_p$, while the functions A, B, and C depend on E_ν, the momentum transfer ($Q^2 = 2M_pT_p$), and form factors of proton. The expressions can be found in Ref. [10]. A more familiar expression for low-energy interactions, in the small-Q^2 limit, is given in Ref. [3]. We retain the Q^2 dependence in our analysis, but note that the impact on the event rates is small.

Due to the large energy loss rate of proton, the scintillation from a recoiled proton is nearly isotropic and the direction of proton (and hence, that of the incident neutrino) is not reconstructed. As a result, the angular distribution of these events is not measurable and we, therefore, only focus on the angle-averaged cross section and flux.

There are two main sources of uncertainty in νp ES cross section: (i) the axial mass parameter M_A, and (ii) contribution of strange sea quarks to the form factors (Δs). For the axial mass parameter, we use the universal average value from neutrino scattering, i.e., $M_A = 1.026 \pm 0.021$ GeV [11]. This results in an uncertainty of less than 5% for $E_\nu \leq 1$ GeV. Moreover, the current estimates for $\Delta s = -0.08 \pm 0.02$ [12] result in an uncertainty of ∼3%. For this analysis, we conservatively assume that the cross section uncertainties are $\mathcal{O}(10\%)$.

For neutrinos and antineutrinos with $E_\nu \geq 550$ MeV, the momentum transfer to proton is large enough for the single-pion production through the delta resonance. However, we expect such processes to have much smaller cross sections than νp ES, and the corresponding event rates can be ignored. The νe ES cross section is relatively smaller, and we can safely ignore these interactions in our analysis.

2. Quenched proton scintillation

Due to photosaturation losses, i.e., quenching, the visible energy ($E_{\rm vis}$) is different from the kinetic energy of the recoiling proton. The differential event spectrum in terms of visible energy is given by

$$\frac{dN}{dE_{\rm vis}} = \left(\frac{dE_{\rm vis}}{dT}\right)^{-1}\frac{dN}{dT}. \tag{3}$$

The visible energy is related to T_p through

$$E_{\rm vis}(T_p) = \int_0^{T_p} \frac{dT}{1 + k_B\langle dE/dx\rangle + k_C\langle dE/dx\rangle^2}, \tag{4}$$

where $k_B = 6.5 \times 10^{-3}$ g/cm^2/MeV and $k_C = 1.5 \times 10^{-6}$ (g/cm^2/MeV)^2 are Birks's constants [13]. The average energy loss during propagation, $\langle dE/dx\rangle$, is

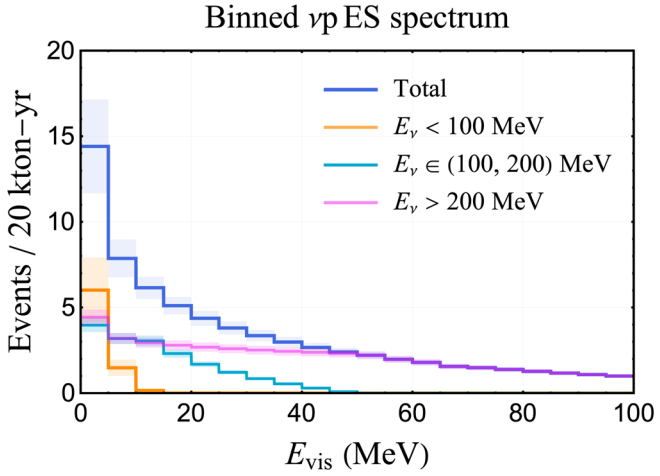

FIG. 1. The binned event spectrum ($\Delta E_{\rm bin} = 5$ MeV) from three energy ranges of the atmospheric neutrino spectrum, and the total spectrum. The shaded regions represent the uncertainties arising from the cross section and flux estimates. Note that the uncertainties are larger in the lower energy bins, mostly because of the uncertain neutrino flux for $E_\nu < 100$ MeV.

determined by the baseline parameters[1,2] of JUNO simulations [6]. Note that the nonlinear but one-to-one mapping between $E_{\rm vis}$ and T_p, and good energy resolution of the detector imply that the effects of quenching can be inverted and one can, in principle, obtain dN/dT_p from $dN/dE_{\rm vis}$. This is useful in reconstructing the incident neutrino spectrum and has been studied in the context of supernova neutrinos [14,15].

3. Predicted νp ES spectrum

The atmospheric neutrinos with $E_\nu \in (100, 200)$ MeV are special, because only the electron-flavor component has been measured through charged current interactions. We ask if the muon and tau flavor components have a detectable imprint on νp ES events spectrum. For this purpose, we take a closer look at the distribution of events from various parts of the atmospheric neutrino spectrum, and divide the flux into three energy ranges:

(1) $E_\nu < 100$ MeV, which has large uncertainties,
(2) $E_\nu \in (100, 200)$ MeV which is partly measured, and
(3) $E_\nu > 200$ MeV, which is well determined.

The event spectrum from these three energy ranges and the total event spectrum, is shown in Fig. 1. We also show the uncertainty in the event spectrum from the cross section as well as flux estimates.

The events from an incident neutrino with energy E_ν are distributed over the range $0 \le T_p \le 2M_p E_\nu^2/(M_p + E_\nu)^2$. As a result, there is a significant contribution to low-energy bins from the high energy part of the atmospheric neutrino spectrum. It seems, *a priori*, that reconstruction of the incident spectrum from νp ES events will be challenging.

From Fig. 1, one notes that in the visible energy range $E_{\rm vis} \in (15, 40)$ MeV, the contribution from neutrinos with $E_\nu \ge 200$ MeV is similar for all the energy bins, whereas the contribution from $E_\nu \in (100, 200)$ MeV decreases with energy. With much larger exposure, this excess of events at low energies can become statistically significant, and if detected, would represent a measurement of the flux of $\nu_\mu + \bar{\nu}_\mu + \nu_\tau + \bar{\nu}_\tau$ for $E_\nu \le 200$ MeV, after statistically subtracting the contribution from $\nu_e + \bar{\nu}_e$. One can also note that the contribution from the flux with $E_\nu < 100$ MeV, which has large uncertainties, is mostly in the low energy bins, and will not be relevant if we have an energy threshold of $E_{\rm vis} \sim 15$ MeV.

C. Singles from νC QEL

The neutral-current interactions of atmospheric neutrinos in JUNO have been studied in Ref. [16]. These interactions are dominated by QEL processes where one or more nucleons can be knocked out of ^{12}C. A detailed study of this process has been carried out in Ref. [16], which reports the event rates for various channels $(1p, 1n, 1p1n, 2p, 2n, ...)$, as well as the recoil proton spectrum from the sum of these channels. The total event rate with at least one proton in the final state[3] is found to be $\sim$30 kton^{-1} yr^{-1}. For 20 kton − yr exposure of JUNO, this implies an aggregate of $\sim$600 events, distributed over $T_p \in (0.1, 300)$ MeV.

We need to estimate the singles event rate from νC QEL process, which arises from the single proton knockout

$$1p\colon\ \nu + {}^{12}\mathrm{C} \to \nu + p + {}^{11}\mathrm{B}^{(*)}, \tag{5}$$

and from multiple proton knockouts such as

$$2p\colon\ \nu + {}^{12}\mathrm{C} \to \nu + 2p + {}^{10}\mathrm{Be}^{(*)}, \tag{6}$$

$$3p\colon\ \nu + {}^{12}\mathrm{C} \to \nu + 3p + {}^{9}\mathrm{Li}^{(*)}. \tag{7}$$

These protons are a part of the total proton spectrum given in Ref. [16]. To isolate the singles events, we calculate the fraction of "proton-only" knockout events that do not have a neutron in the final state. Using the results in Ref. [16], we find that

$$\frac{N_{1p} + N_{2p} + N_{3p} + \cdots}{N_{1p} + N_{1p1n} + N_{2p} + N_{1p2n} + N_{2p1n} + \cdots} \approx 0.52, \tag{8}$$

[1] $\langle dE/dx\rangle \approx 0.88\langle dE/dx\rangle_C + 0.12\langle dE/dx\rangle_H$.
[2] The energy loss rate on carbon and hydrogen can be obtained from www.physics.nist.gov/PhysRefData/Star/Text/PSTAR.html.
[3] This can be obtained by adding histograms given in Fig. 4 of Ref. [16] as well as integrating the spectrum in Fig. 6 of Ref. [16].

which implies that roughly half of the protons do not have a neutron tag. Therefore, the singles spectrum from νC QEL interaction can be approximated by scaling the proton spectrum given in [16] by 0.52. The $E_{\rm vis}$ distribution is obtained by applying the effects of quenching using Eq. (3).

The daughter nuclei in a QEL process can deexcite through protons and/or alpha particle emission. However, these particles are estimated to be lower in number, and most of them have kinetic energies below 20 MeV [16]. We estimate the secondary particle contamination of LES sample to be less than two events per 20 kton − yr. Moreover, after deexcitation, some of the channels result in unstable nuclei with short lifetimes that undergo β decay. These β decays can be used to tag the proton scintillation events, as has been demonstrated in Ref. [17]. While this will allow us to identify a fraction of the LES sample as coming from νC QEL, we do not use this information in our analysis. It is also possible that the elastic scatterings between a knockout neutron and free proton in detector results in visible scintillation. However, these events will be vetoed by the accompanying neutron capture.

The event rate predictions in Ref. [16] depend on the choice of Monte Carlo generator for neutrino interactions. In Fig. 2, we show the expected rate of νC QEL singles at JUNO, as predicted by the neutrino event generators GENIE [18] and NuWro [19]. It appears that νC QEL predictions are sensitive to details of the nuclear structure, unlike the robust predictions for νp ES. For our analysis in the rest of the paper, we use the results obtained by GENIE [18], with 10% uncertainty.

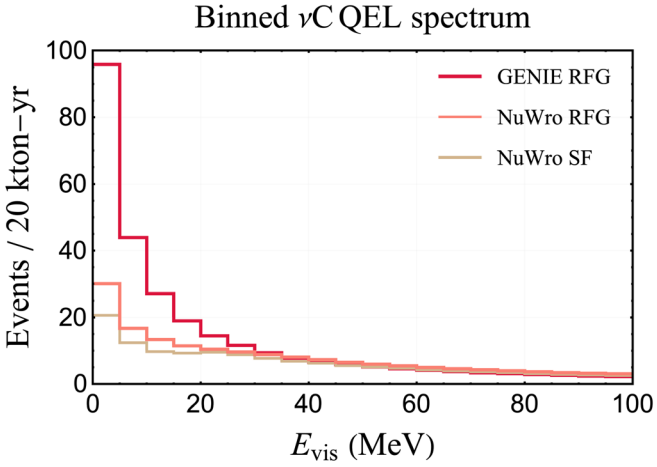

FIG. 2. The binned energy distribution of singles ($\Delta E_{\rm bin} = 5$ MeV) from νC QEL interactions is shown for different neutrino interaction Monte Carlo (MC) generators [GENIE and NuWRO with nuclear structure models—relativistic Fermi gas (RFG) and spectral function approach (SF)].

III. BACKGROUNDS AND THRESHOLD

A. Cosmic muon spallation

The passage of cosmic muons through the detector produces isotopes through spallation. These unstable isotopes decay in the detector, and their daughter particles can lead to visible signals. The singles background (i.e., without an associated neutron capture) originates from $\beta^{\pm}$, $\beta^{\pm}\gamma$, $\beta^{\pm}p$, and $\beta^{\pm}\alpha$ decays of these cosmogenic isotopes. The βn decays do not contribute to singles as the neutron can be tagged.

The cosmic muon spallation and isotope yields have been extensively studied for Super-Kamiokande in Refs. [20–22]. The liquid scintillator detector KamLAND has measured the yields of some cosmogenic isotopes [23]. Since the average muon energy at the JUNO site is lower than that at KamLAND,[4] the isotope yields at JUNO would be nearly 90% of that at KamLAND [6]. In this paper, we scale the measured KamLAND yields to JUNO where available, and, for other cosmogenic isotopes, we use simulation yields from Table 13–9 in Ref. [6]. The isotope yields and other details are given in Table I.

1. Decay of cosmogenic isotopes

To predict the visible-energy distribution of singles from cosmogenic isotopes, we estimate their production rate in the detector. Looking at their half-lives (cf., Table I), it is reasonable to assume that all the cosmogenic isotopes would decay within a day. The production count per day (CPD) of the radio isotope i is given as

$$\mathrm{CPD}_i = Y_i R_\mu T \rho \langle L_\mu \rangle, \tag{9}$$

where Y_i is the isotope yield, $R_\mu = 3$ Hz is the rate of cosmic ray muons traversing through in JUNO, $T = 86400$ s is the time interval, and $\langle L_\mu \rangle \approx 23$ m is the average muon track length in JUNO [6]. These values give a more useful and simplified expression

$$\mathrm{CPD}_i = \frac{47.7}{\mathrm{day}} \left(\frac{Y_i}{10^{-7}\ \mathrm{muon^{-1}\ g^{-1}\ cm^2}} \right), \tag{10}$$

which we use in the evaluation of the event rate $R_i = \mathcal{B}_i \times \mathrm{CPD}_i$, as well as the event spectrum

$$\frac{dN_i}{dE_{\rm vis}} = \mathcal{B}_i \times \mathrm{CPD}_i \times f_i(E_{\rm vis}). \tag{11}$$

Here $\mathcal{B}_i$ is the branching ratio of the isotope to the singles channels, and f_i is the normalized distribution of $E_{\rm vis}$ for the ith isotope.[5] As the individual isotopes cannot be

[4] $\langle E_\mu \rangle \sim 215$ GeV for JUNO [6], and $\langle E_\mu \rangle \sim 260$ GeV for KamLAND [23].

[5] The normalized distribution can be obtained from www-nds.iaea.org/relnsd/vcharthtml/VChartHTML.html, which uses BetaShape [24].

identified, only the cumulative event spectrum from these isotopes can be measured.

2. Veto criterion

The cosmogenic isotopes that decay within a few seconds of the muon passage can be tagged, and the events can be removed by imposing appropriate spatial and temporal cuts. This was demonstrated for Super-Kamiokande in Ref. [21]. By accounting for the muon energy deposition along the track, it was proposed to veto a small cylindrical volume centered around the muon track. A similarly detailed analysis for JUNO is required, but it is beyond the scope of this paper. To get rid of cosmogenic isotope decays, we propose a much more conservative veto—a cylindrical volume around the entire track of the cosmic muon with radius $R_{\rm veto}$ for a time $\Delta t_{\rm veto}$. This results in a dead volume fraction of

$$\frac{\delta V}{V} \sim \frac{(R_\mu \Delta t_{\rm veto}) \times \pi R_{\rm veto}^2 \langle L_\mu \rangle}{\frac{4}{3}\pi R_{\rm CD}^3}, \tag{12}$$

where $R_{\rm CD} = 17.7$ m is radius of the central detector and $\langle L_\mu \rangle \approx 23$ m is the average muon track length in JUNO [6]. For $R_{\rm veto} = 3$ m and $\Delta t_{\rm veto} = 1.2$ s (similar to Ref. [6]), the dead volume fraction is ∼10%, whereas for $\Delta t_{\rm veto} = 2$ s, the dead volume fraction increases to ∼17%. We envision that this dead volume fraction of detector will be compensated by longer duration of data taking, to get the appropriate effective exposure.

Note that, these estimates do not account for the muon tagging and track reconstruction efficiencies. A detailed Monte Carlo simulation, which also accounts for detector systematics, is required to optimize the veto criterion. In Ref. [6], similar cuts were proposed to identify the inverse beta-decay events in JUNO, with additional cuts to tag the neutron capture.

3. Irreducible background and threshold

The fraction of cosmogenic isotopes that decay outside the $\Delta t_{\rm veto}$ window cannot be tagged, and constitute the irreducible background. The effective rate of background events from a cosmogenic isotope is given by

$$\tilde{R}_i = e^{-\Delta t_{\rm veto}/\tau_i} \times \mathcal{B}_i \times {\rm CPD}_i, \tag{13}$$

which is provided in Table I. The effective event spectrum is estimated by

$$\frac{dN_i}{dE_{\rm vis}} = e^{-\Delta t_{\rm veto}/\tau_i} \times \mathcal{B}_i \times {\rm CPD}_i \times f_i(E_{\rm vis}). \tag{14}$$

TABLE I. The details of the cosmogenic isotopes considered in this paper is tabulated. The end point of the beta spectrum ($E_\beta^{\rm max}$) and the half-life $T_{1/2}$ were obtained from www-nds.iaea.org. The experimentally measured yields by KamLAND [23] have been scaled to obtain the yields in JUNO. Wherever KamLAND measurements are not available, results of JUNO simulations [6] have been used. The isotope production CPD from Eq. (9) captures the number of isotopes that are produced in the detector per day. The fraction of these isotopes that decay outside the $\Delta t_{\rm veto} = 2$ s constitute the irreducible background, whose rate $\tilde{R}$ [using Eq. (13)] is tabulated.

Radio isotope	$E_\beta^{\rm max}$ (MeV)	$T_{1/2}$ (s)	Yield ($10^{-7}\mu^{-1}g^{-1}$ cm^2) for KamLAND (Ref. [23])	Yield ($10^{-7}\mu^{-1}g^{-1}$ cm^2) for JUNO (this work)	CPD (per day)	$\tilde{R}$ (per day)
^{14}B	20.64	0.0126	⋯	4.4×10^{-3}	0.021	∼0
^{12}N	16.32	0.0011	1.8 ± 0.4	1.62	77.3	∼0
^{9}C	15.47	0.126	3.0 ± 1.2	2.7	128.8	0.002
^{8}B	13.9	0.770	8.4 ± 2.4	7.56	360.6	59.61
^{9}Li	13.60	0.178	2.2 ± 0.2	1.98	94.4	0.019
^{13}B	13.43	0.0174	⋯	0.251	12	∼0
^{12}B	13.37	0.0202	42.9 ± 3.3	38.6	1841.4	∼0
^{8}Li	12.97	0.839	12.2 ± 2.6	10.98	523.7	100.38
^{18}N	11.92	0.62	⋯	1.88×10^{-4}	0.009	0.001
^{12}Be	11.71	0.0215	⋯	9.43×10^{-3}	0.45	∼0
^{11}Be	11.51	13.76	1.1 ± 0.2	0.99	47.2	42.67
^{16}N	10.42	7.13	⋯	0.273	13	10.70
^{15}C	9.77	2.449	⋯	1.26×10^{-2}	0.6	0.34
^{8}He	9.67	0.119	0.7 ± 0.4	0.63	30.0	∼0
^{17}N	8.68	4.173	⋯	8.8×10^{-3}	0.42	0.015
^{6}He	3.51	0.80	⋯	11.40	544	97.657
^{10}C	1.91	0.747	16.5 ± 1.9	14.85	708.35	110.77
^{13}N	1.198	597	⋯	0.398	19	18.96
^{11}C	0.96	1221	866 ± 153	779	37177	377134

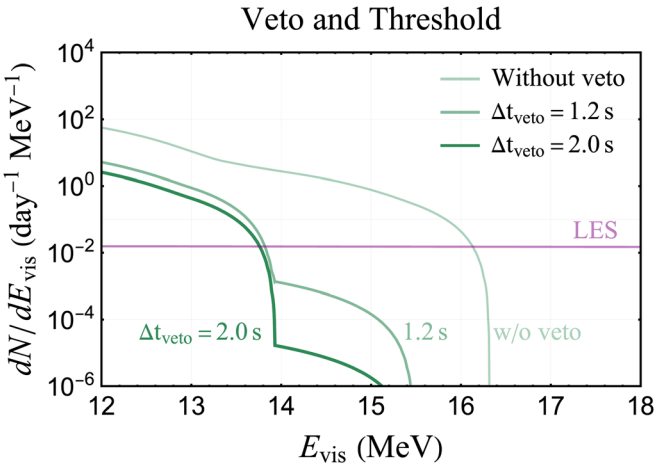

FIG. 3. The cumulative event spectrum from the cosmogenic isotope decay for $\Delta t_{veto} = 0$ s (equivalent to without veto), 1.2 s, and 2.0 s. We show the LES spectrum with light-purple curve for comparison. We will take $\Delta t_{veto} = 2.0$ s as our benchmark.

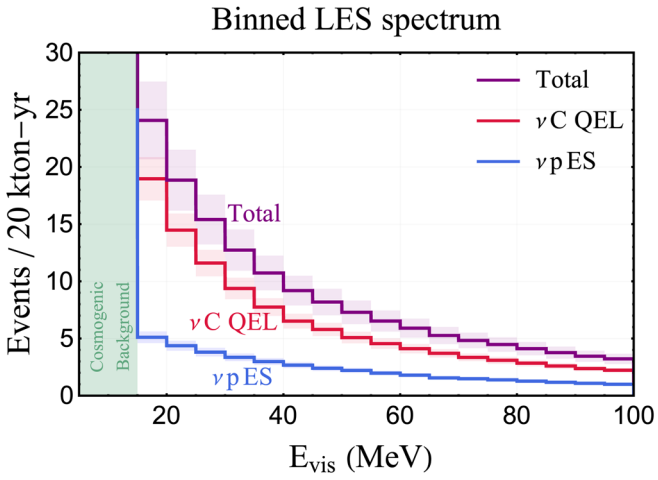

FIG. 4. The binned event-rate spectrum for νp ES (blue) and proton knockouts from νC QEL interactions (red) are shown. The cumulative spectrum from both the channels is shown in purple. The green shaded region below 15 MeV represents the overwhelming background from cosmogenic isotope decay.

In Fig. 3, we have shown the cumulative event spectrum from cosmogenic isotope decay for $\Delta t_{veto} = 0$ s (equivalent to without veto), 1.2 s, and 2.0 s. For details, please refer to Fig. 8 in the Appendix. Without any veto, the cosmogenic isotope decays constitute a wall-like background at $E_{vis} \sim 16.5$ MeV. Our veto criterion, with $\Delta t_{veto} = 2$ s, allows us to lower the threshold up to 14 MeV. We present our results with a conservative threshold of 15 MeV. Note that, by considering the energy deposition along the track, the length of the cylindrical volume veto can be reduced and Δt_{veto} can be increased with little change to dead volume fraction. This significantly reduces the cosmogenic backgrounds [21].

B. Other backgrounds

The other known singles backgrounds include intrinsic radioactivity and reactor neutrinos. However, these neutrinos contribute for $E_{vis} \leq 10$ MeV. As cosmogenic backgrounds already overwhelm the signal at these energies, we do not discuss them in detail.

Incomplete reconstruction of events, e.g., missing one or more final state particles, can lead to LES events. For example, a low-energy atmospheric $\bar{\nu}_e$ interacting via charged current produces a positron and a neutron; if the neutron is not tagged this can contribute to an LES event. However, for the $E_{vis} \in (15\text{–}100)$ MeV window considered for LES events, the relevant low-energy $\bar{\nu}_e$ have a small event rate. Therefore we expect such backgrounds to be small. The event rate for inverse beta decay from diffuse supernova background neutrinos is estimated to be 1.8–3.4 per 20 kton − yr for $\langle E_\nu \rangle \in (12, 21)$ MeV [6]. Even among these, only the events with a missed neutron tag will contribute to LES, which we expect to be negligible. Another possibility arises from neutrino-carbon interaction resulting in an on shell Δ baryon, which decays to a hadron and a pion. The protons from this Δ-resonance channel typically lead to $E_{vis} > 200$ MeV, and will not be part of the LES sample. Only the pions with mis(under) reconstructed energy and missed neutron tag will contribute to the LES sample, and we expect their event rates to be small. However, a detailed study of the detector efficiencies and reconstruction is warranted.

IV. FORECAST FOR JUNO-LES

It is clear that the low-energy singles spectrum at JUNO will be dominated by irreducible cosmogenic isotope decay, intrinsic radioactivity, solar and reactor neutrinos. Above 15 MeV visible energy, the events dominantly arise from νp ES and νC QEL interactions. This JUNO-LES sample will provide evidence of neutral-current interactions of atmospheric neutrinos. In Fig. 4, we have shown our estimate for the binned event spectrum for $E_{vis} \in (15, 100)$ MeV from νp ES, νC QEL, and the "total" sum of the two. There are a few events expected above 100 MeV, but we do not include them in our counting. For 20 kton − yr exposure, we expect ~40 events from νp ES, and ~108 events from νC QEL. Therefore, we expect a total of ~148 events with $E_{vis} \in (15, 100)$ MeV in the JUNO-LES sample.

The first goal of JUNO would be to establish the existence of LES events, and therefore, the neutral current interactions of atmospheric neutrinos. In this analysis, the backgrounds for $E_{vis} \geq 15$ MeV have been assumed to be negligible. Therefore, the first LES events may be observed with a few tenths of kton-yr exposure, according to our estimations. If we further want to claim a discovery of νp

ES events above the "background" of νC QEL events, then we need a larger exposure. Assuming only statistical errors[6] and no other background, we estimate that JUNO can discover νp ES at 3σ (5σ) with 12 (34) kton-yr exposure. Note that, these estimates are only based on the counting of events, and more detailed analysis can be performed which also accounts for the energy distributions of the νp ES and νC QEL events.

V. SENSITIVITY TO NEW PHYSICS

Measurement of the LES sample at JUNO will open the window to testing many new physics scenarios. In this section, we first show that interesting limits can be obtained using model-independent analysis. Later, through two examples, we will also show how one can obtain model-dependent limits on possible fluxes of energetic new particles.[7]

A. Model independent limits

A flux of "beyond standard model" particles ψ can arise from the annihilation/decay of galactic or solar dark matter [26–29]. They can also be emitted during evaporation of the primordial black holes [30,31]. These particles can also be produced in astrophysical processes or through cosmic ray interactions [32–50]. We choose to remain independent of the production mechanism and assume a flux of boosted ($E > m$) particles with monochromatic energy spectrum. The flux at a detector can be written as

$$\frac{d\phi_\psi}{dE} = \phi_0 \delta(E - E_\psi), \tag{15}$$

where ϕ_0 is the normalization in units of $\mathrm{cm}^{-2}\,\mathrm{sec}^{-1}$ and E_ψ is the energy of the boosted particle. If this flux arises from dark matter annihilation ($\mathrm{DM} + \mathrm{DM} \to \psi + \psi$) or decay ($DM \to \psi\psi$), then $E_\psi = M_{\mathrm{DM}}$ or $E_\psi = M_{\mathrm{DM}}/2$, respectively.

The boosted particle would be detected through elastic scattering with protons in the detector ($\psi + p \to \psi + p$). The cross section for this process depends on the details of the particle physics model. We consider two benchmark scenarios for the mediator—heavy and light, and two models for the interaction—vector and axial vector. Given the typical momentum transfers, mediator masses below 20 MeV can be considered as light.

For the heavy mediator case, one is only sensitive to a ratio of coupling strength (g_{H}) and the mediator mass ($M_{Z'}$). On the other hand, for the light mediator case, one is only sensitive to the coupling strength. In order to compare quantities with the same dimensions, for the light mediator scenario we take the heavy scale (corresponding to $M_{Z'}$ above) to be the mass of proton. As a result, the strength of interaction in these two scenarios is captured by an effective parameter

$$G_{\mathrm{eff}} = \begin{cases} \frac{g_{\mathrm{H}}^2}{8M_{Z'}^2} c_{V/A} & [\text{Heavy mediator(HM)}] \\ \frac{g_{\mathrm{L}}^2}{8M_p^2} c_{V/A} & [\text{Light mediator(LM)}] \end{cases}, \tag{16}$$

where $c_{V(A)} = 0.04(0.64)$ arises from the form factors of proton. The differential cross section for ψp ES is

$$\frac{d\sigma_{\psi p}}{dT_p} = \begin{cases} G_{\mathrm{eff}}^2 \frac{M_p}{\pi}\left(1 \pm \frac{M_p T_p}{2E_\psi^2}\right) & [\mathrm{HM}] \\ G_{\mathrm{eff}}^2 \frac{M_p}{\pi}\left(1 \pm \frac{M_p T_p}{2E_\psi^2}\right) \times \frac{M_p^2}{4T_p^2} & [\mathrm{LM}] \end{cases}, \tag{17}$$

where $-(+)$ are for vector (axial-vector) current.

We can now compute the quenched proton spectrum from ψp ES. The event rate depends on E_ψ and the product $\phi_0 \times G_{\mathrm{eff}}^2$. To obtain the 90% confidence limits (C.L.) sensitivity of JUNO to the flux of these boosted particles, we consider the events from ψp ES as signal and the total Standard Model LES events as the background. As the spectrum from both interactions is predictable, a bin-by-bin comparison will lead to better sensitivity, but is not required for our simple analysis. The boosted particle parameter space that can be probed by JUNO is shown in Fig. 5. We find that the event rate is higher for light mediator scenario and axial-vector current interaction, as expected.

The volume of KamLAND is 0.697 kton. Using a fiducial exposure of 123 kton-day, KamLAND has reported one event with $E_{\mathrm{vis}} \in (13.5, 20)$ MeV which is consistent

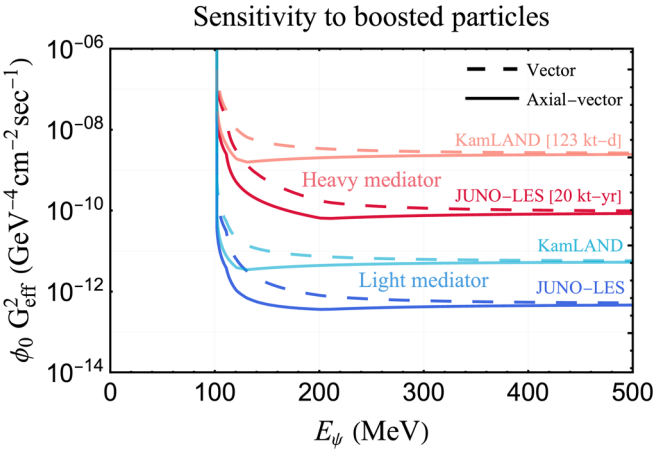

FIG. 5. The 90% C.L. discovery sensitivity of JUNO-LES with 20 kton − yr exposure to the parameters of the monochromatic boosted particle flux is shown for heavy (light) mediator case by red (blue) curves. The solid (dashed) curve represents the axial-vector (vector) current mediation. The 90% C.L. exclusion limits obtained from KamLAND with 123 kton-day exposure [5] is shown with lighter shades.

[6]We use the figure of merit $S/\sqrt{B}$ as a measure of discovery sensitivity, and $S/\sqrt{S+B}$ to obtain exclusion limits [25].

[7]Novel interactions can also modify the νp ES cross section itself, which we do not study here.

with their estimate for background [5]. The nonobservation of excess events in this bin allows us to put 90% C.L. exclusion limits on the flux of boosted particles. These limits for the various cases are shown in Fig. 5. The projected sensitivity of JUNO is ∼100 times more than KamLAND due to larger exposure and a wider $E_{\rm vis}$ range of the LES sample.

B. Dark matter annihilating to sterile neutrinos

One of the simplest extensions to the Standard Model is a neutral fermion called sterile neutrino (ν_s), which can also act as a portal to dark matter. In these models, the annihilation of dark matter is dominated by $\chi\chi \to \nu_s\nu_s$ which determines the relic density [27–29]. If the mixing angle between sterile and active neutrino is large (∼0.1), the flux of sterile neutrinos will be accompanied by a flux of active neutrinos, albeit smaller, which can be detected. However, if the mixing angle is small ($< 10^{-3}$), the flux of active neutrinos will be too small to be detected and one must rely on the detection of ν_s. One of the possibilities is to detect $\nu_s p$ elastic scattering ($\nu_s + p \to \nu_s + p$) in the LES sample at JUNO.

The flux of sterile neutrinos from s-channel annihilation of galactic dark matter is given by

$$\frac{d\phi}{dE} = \frac{1}{4\pi}\frac{\langle\sigma v\rangle}{M_\chi^2}\delta(E - M_\chi)\mathcal{J}, \tag{18}$$

where $\mathcal{J} = 2.3 \times 10^{23}$ GeV^2 cm^{-5} is the all-sky J factor [51], and $\langle\sigma v\rangle$ is the thermal averaged cross section adapted from Ref. [52]. We have assumed the dark matter to be a Majorana fermion. In case it were a Dirac fermion, the flux would smaller by a factor of two. To obtain conservative estimates, we ignore the contribution to flux arising from the extragalactic component. We also assume that $\nu_s p$ ES is mediated by a light vector boson, and take the coupling $g_{\rm L} = 0.1$ for illustration.

The parameter space excluded by KamLAND data, and the 90% C.L. discovery sensitivity of the LES sample at JUNO with 20 kton − yr exposure are shown in Fig. 6. We also show the thermal averaged cross section for obtaining the correct relic abundance, and find that JUNO can probe this model for dark matter mass in the range 100 MeV to a few GeV. We also show the exclusion limits from Super-Kamiokande and the projected sensitivity of DUNE and Hyper-Kamiokande for dark matter annihilation to active neutrinos, relevant when the mixing angle between active and sterile neutrino is large. Note that the above limits were calculated assuming a light mediator. For a given value of M_χ, the limits for the heavy mediator case can be obtained using Eq. (16), which gives the substitution rule

$$\frac{g_{\rm L}^4}{M_p^4}\langle\sigma v\rangle_{\rm L} \leftrightarrow \frac{g_{\rm H}^4}{M_{Z'}^4}\langle\sigma v\rangle_{\rm H}, \tag{19}$$

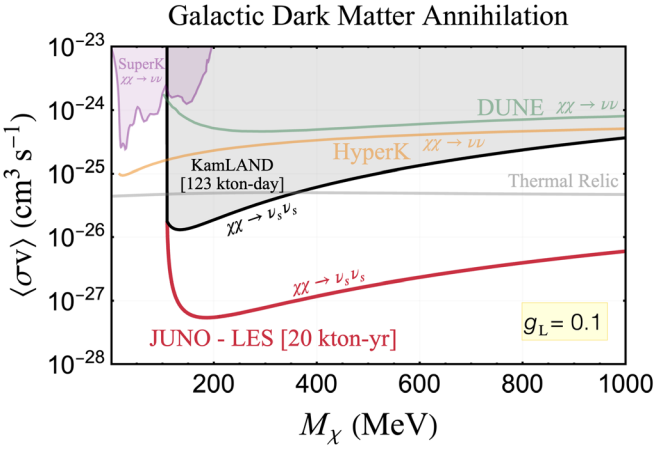

FIG. 6. The 90% C.L. exclusions limit from KamLAND [5], and discovery sensitivity of JUNO to the parameters of dark matter annihilation to sterile neutrino, assuming light mediator and $g_{\rm L} = 0.1$. The parameter space above the red curve would result in detectable events in the JUNO-LES sample with an exposure of 20 kton − yr. The gray curve shows the thermal rate required for obtaining the observed dark matter abundance. For comparison, we show the exclusion limit from Super-Kamiokande obtained from dark matter annihilation to neutrinos [51,53]. We also show the projected sensitivity from DUNE [51] and Hyper-Kamiokande [54] to the active neutrino channel. These are relevant for the case of large mixing angle between active and sterile neutrino.

where the subscript L (H) denotes the parameters in the light (heavy) mediator scenario.

C. Boosted dark matter

The elastic scattering between dark matter and proton ($\chi + p \to \chi + p$) in scintillator detector like JUNO will lead to a singles event from the scintillation signal of the recoiled proton. In general, the momentum transfer to protons from the scattering with cold and nonrelativistic dark matter is small, quenched, and cannot be detected. However, the interaction of cosmic rays on galactic dark matter can boost these particles to higher velocities, which allows for larger momentum transfers in a detector [33,34]. In Ref. [55], constraints on the interaction cross section $\sigma_{\chi p}$ and the mass of dark matter M_χ were obtained from neutrino experiments. The sensitivity of JUNO was projected by appropriate scaling of KamLand data. The LES spectrum computed in this paper will act as a background in the search for such boosted dark matter. We recalculate the projected sensitivity of JUNO to $\sigma_{\chi p}$ in the light of the LES background.

We follow the method of [33] to estimate the flux of boosted dark matter. We compute the total number of events with $E_{\rm vis} \in (15, 100)$ MeV, and obtain the 90% C.L. discovery sensitivity of JUNO by comparing with the total events in the LES sample, which we consider as background. The results are shown in Fig. 7 along with other

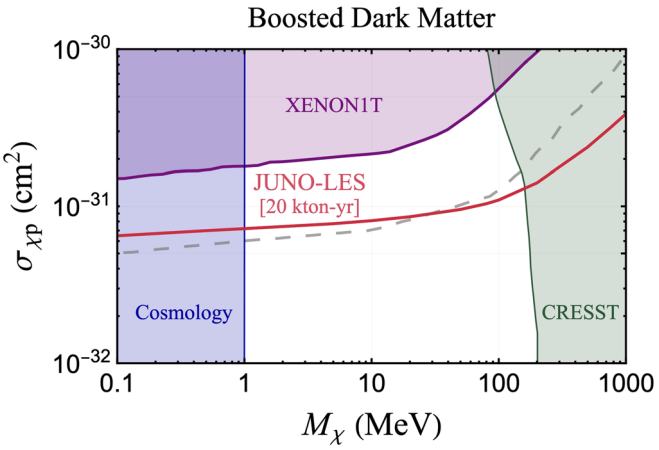

FIG. 7. The 90% C.L. discovery sensitivity with the JUNO-LES 20 kton − yr sample to the parameters of boosted dark matter is shown in red. The gray dashed line is the corresponding estimate from Ref. [55]. The exclusion limits from XENON1T and other direct detection experiments are adapted from [33,34]. The limit from cosmology is taken from [56].

relevant limits. Our projected sensitivity is mostly consistent with the ones obtained in Ref. [55].

VI. SUMMARY AND OUTLOOK

The neutral-current interactions of atmospheric neutrinos in a large volume liquid scintillator detector, such as JUNO, is mainly through ES on protons and QEL scattering on carbon nuclei. The recoiled protons are detected through their scintillation signal. Such prompt-only events are also called as "singles." In this paper, we predict the visible energy distribution of singles at JUNO, due to atmospheric neutrino interactions through the νp ES and νC QEL channels.

We determine the background due to cosmogenic isotope decay, which would dominate for $E_{\rm vis} \leq 16.5$ MeV. Using veto on singles in the vicinity of a muon track, we show that the threshold may be reduced to $E_{\rm vis} \sim 15$ MeV, above which the atmospheric neutrino signal dominates. Based on our estimates, we propose that JUNO can maintain a LES database (i.e., $E_{\rm vis} \geq 15$ MeV and no delayed neutron capture signal) wherein the neutral-current interactions of atmospheric neutrinos can be detected. The main results of this paper are shown in Fig. 4.

The first goal with the LES events would be to establish their existence, and therefore ensure the detection of neutral-current interactions of low-energy atmospheric neutrinos. Assuming only statistical errors and no other background, we expect JUNO would discover these events with the exposure of a few tenths kton-yr. The next step would be a confirmed detection of νp ES events, which is a robust prediction of Standard Model with small uncertainties. We estimate that JUNO can find evidence of νp ES by rejecting the QEL-only hypothesis at 3σ (5σ) with 12 (34) kton-yr exposure.

The LES database can also probe new physics scenarios, which can give rise to singles in the detector. The LES sample is particularly advantageous if the new physics model does not admit charged-current-like interactions, for example, in the case of boosted dark sector particles. We have estimated the discovery sensitivity of the LES sample for such scenarios. We also estimate the discovery sensitivity for two well-motivated new physics scenarios—dark matter annihilation to sterile neutrinos, and boosted dark matter. In principle, the LES sample would also be sensitive to neutral-current nonstandard interactions that modify the predictions of νp ES and νC QEL channels. However, we have not considered this possibility in this work.

The estimates obtained in the paper are promising. Future work with detailed studies of neutrino interactions in the JUNO detector will shed more light on backgrounds, and aid in developing mitigation techniques. We look forward to a detailed study of the muon spallation at JUNO, and veto analysis including pulse shape discrimination. This will allow for a lower threshold, and therefore, enhance the prospects for the detection of low-energy atmospheric neutrinos and possible new physics signals.

ACKNOWLEDGMENTS

B. C. would like to acknowledge private correspondence with Jie Cheng regarding the results of their paper. A. D. would like to thank S. Agarwalla for useful discussions. The work of B. D. and A. D. are supported by the Department of Atomic Energy (Government of India) research project under Project Identification No. RTI 4002. B. D. is also supported by a Swarnajayanti Fellowship of the Department of Science and Technology (Government of India), and by the Max-Planck-Gesellschaft through a Max Planck Partner Group.

APPENDIX: SUPPLEMENTARY PLOTS—VETOING COSMOGENIC BACKGROUNDS

The decay of cosmogenic isotopes is a major background for visible energy in the range of tens of MeV. In Fig. 8, we show the contribution of various radio-isotopes to the cosmogenic background with and without veto. The aggregate of these contributions appears as the cosmogenic background in Fig. 3.

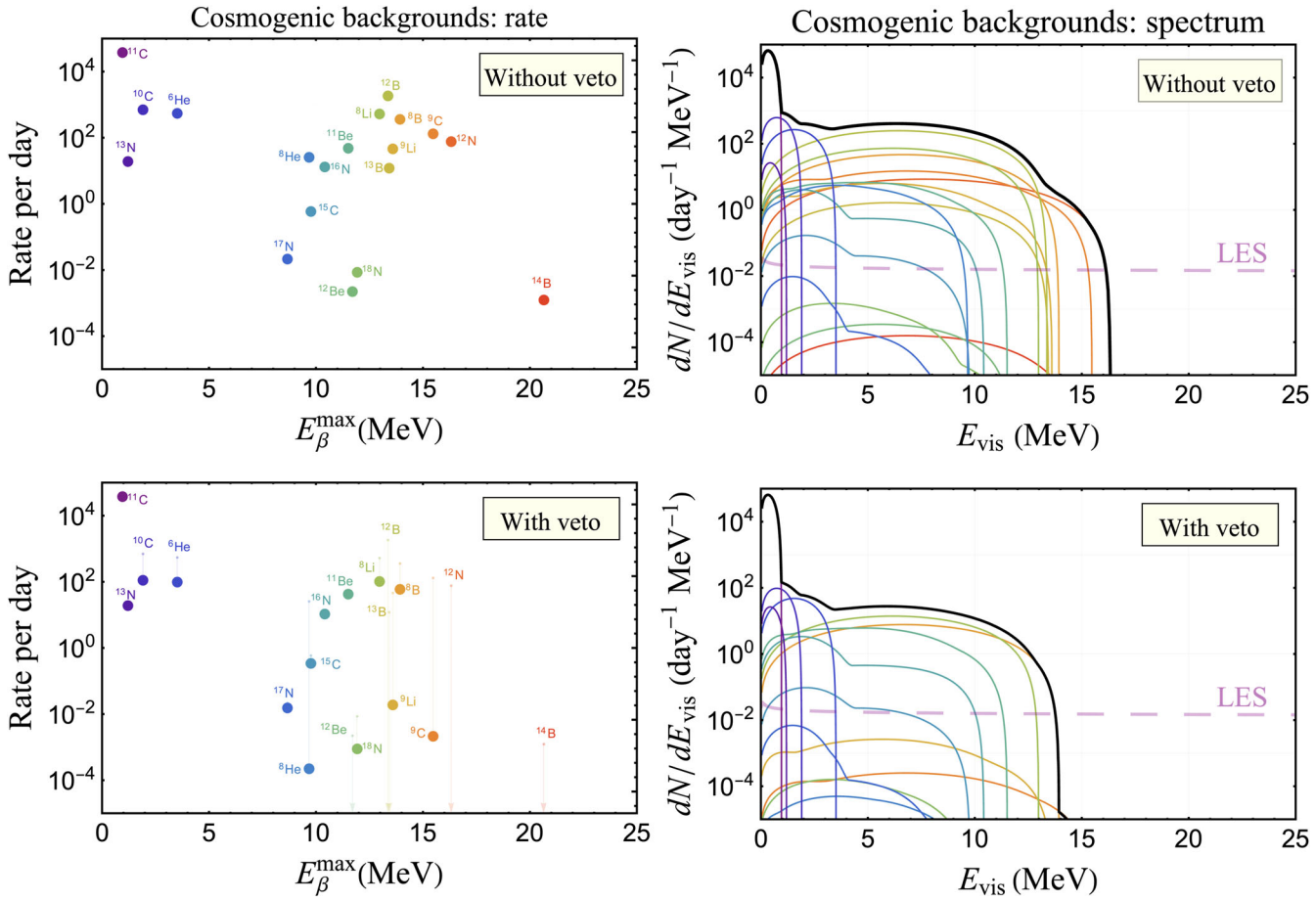

FIG. 8. Left: the event rate per day for the cosmogenic isotopes is shown against the end point of their beta decay spectrum without (top) and with (bottom) $\Delta t_{\rm veto} = 2$ s. Right: the singles spectrum from decays of cosmogenic isotopes without (top) and with (bottom) $\Delta t_{\rm veto} = 2$ s. The color convention is such that the isotopes with lower (higher) $E_\beta^{\max}$ are shown with blue (red) shades. The black curve represents the total cosmogenic background. We have also shown the LES spectrum with dashed light-purple curve for comparison.

[1] Y. Fukuda *et al.* (Super-Kamiokande Collaboration), Evidence for Oscillation of Atmospheric Neutrinos, Phys. Rev. Lett. **81**, 1562 (1998).

[2] John F. Beacom and Sergio Palomares-Ruiz, Neutral current atmospheric neutrino flux measurement using neutrino proton elastic scattering in Super-Kamiokande, Phys. Rev. D **67**, 093001 (2003).

[3] John F. Beacom, Will M. Farr, and Petr Vogel, Detection of supernova neutrinos by neutrino proton elastic scattering, Phys. Rev. D **66**, 033001 (2002).

[4] V. S. Atroshchenko and E. A. Litvinovich, Estimation of atmospheric neutrinos background in Borexino, J. Phys. Conf. Ser. **675**, 012014 (2016).

[5] S. Abe *et al.* (KamLAND Collaboration), Measurement of the 8B solar neutrino flux with the KamLAND liquid scintillator detector, Phys. Rev. C **84**, 035804 (2011).

[6] Fengpeng An *et al.* (JUNO Collaboration), Neutrino physics with JUNO, J. Phys. G **43**, 030401 (2016).

[7] Angel Abusleme *et al.* (JUNO Collaboration), Measuring low energy atmospheric neutrino spectra with the JUNO detector, Eur. Phys. J. C **81**, 10 (2021).

[8] M. Honda, M. Sajjad Athar, T. Kajita, K. Kasahara, and S. Midorikawa, Atmospheric neutrino flux calculation using the NRLMSISE-00 atmospheric model, Phys. Rev. D **92**, 023004 (2015).

[9] G. Battistoni, A. Ferrari, T. Montaruli, and P. R. Sala, The atmospheric neutrino flux below 100-MeV: The FLUKA results, Astropart. Phys. **23**, 526 (2005).

[10] L. A. Ahrens *et al.*, Measurement of neutrino—proton and anti-neutrino—proton elastic scattering, Phys. Rev. D **35**, 785 (1987).

[11] Veronique Bernard, Latifa Elouadrhiri, and Ulf-G. Meissner, Axial structure of the nucleon: Topical review, J. Phys. G **28**, R1 (2002).

[12] F. E. Maas and K. D. Paschke, Strange nucleon form-factors, Prog. Part. Nucl. Phys. **95**, 209 (2017).

[13] J. B. Birks, Scintillations from organic crystals: Specific fluorescence and relative response to different radiations, Proc. Phys. Soc. London Sect. A **64**, 874 (1951).
[14] Basudeb Dasgupta and John F. Beacom, Reconstruction of supernova ν_μ, ν_τ, anti-ν_μ, and anti-ν_τ neutrino spectra at scintillator detectors, Phys. Rev. D **83**, 113006 (2011).
[15] Hui-Ling Li, Xin Huang, Yu-Feng Li, Liang-Jian Wen, and Shun Zhou, Model-independent approach to the reconstruction of multiflavor supernova neutrino energy spectra, Phys. Rev. D **99**, 123009 (2019).
[16] Jie Cheng, Yu-Feng Li, Liang-Jian Wen, and Shun Zhou, Neutral-current background induced by atmospheric neutrinos at large liquid-scintillator detectors: I. model predictions, Phys. Rev. D **103**, 053001 (2021).
[17] Jie Cheng, Yu-Feng Li, Hao-Qi Lu, and Liang-Jian Wen, Neutral-current background induced by atmospheric neutrinos at large liquid-scintillator detectors. II. Methodology for *insitu* measurements, Phys. Rev. D **103**, 053002 (2021).
[18] C. Andreopoulos *et al.*, The GENIE neutrino Monte Carlo generator, Nucl. Instrum. Methods Phys. Res., Sect. A **614**, 87 (2010).
[19] T. Golan, J. T. Sobczyk, and J. Zmuda, NuWro: The Wroclaw Monte Carlo generator of neutrino interactions, Nucl. Phys. B, Proc. Suppl. **229–232**, 499 (2012).
[20] Shirley Weishi Li and John F. Beacom, First calculation of cosmic-ray muon spallation backgrounds for MeV astrophysical neutrino signals in Super-Kamiokande, Phys. Rev. C **89**, 045801 (2014).
[21] Shirley Weishi Li and John F. Beacom, Spallation backgrounds in Super-Kamiokande are made in muon-induced showers, Phys. Rev. D **91**, 105005 (2015).
[22] Shirley Weishi Li and John F. Beacom, Tagging spallation backgrounds with showers in water-Cherenkov detectors, Phys. Rev. D **92**, 105033 (2015).
[23] S. Abe *et al.* (KamLAND Collaboration), Production of radioactive isotopes through cosmic muon spallation in KamLAND, Phys. Rev. C **81**, 025807 (2010).
[24] X. Mougeot, Reliability of usual assumptions in the calculation of β and ν spectra, Phys. Rev. C **91**, 055504 (2015); **92**, 059902(E) (2015).
[25] P. A. Zyla *et al.* (Particle Data Group), Review of particle physics, Prog. Theor. Exp. Phys. **2020**, 083C01 (2020).
[26] Kohta Murase and Ian M. Shoemaker, Detecting asymmetric dark matter in the Sun with neutrinos, Phys. Rev. D **94**, 063512 (2016).
[27] David McKeen and Nirmal Raj, Monochromatic dark neutrinos and boosted dark matter in noble liquid direct detection, Phys. Rev. D **99**, 103003 (2019).
[28] Doojin Kim, Pedro A. N. Machado, Jong-Chul Park, and Seodong Shin, Optimizing energetic light dark matter searches in dark matter and neutrino experiments, J. High Energy Phys. 07 (2020) 057.
[29] Kevin J. Kelly and Yue Zhang, Mononeutrino at DUNE: New signals from neutrinophilic thermal dark matter, Phys. Rev. D **99**, 055034 (2019).
[30] Roberta Calabrese, Marco Chianese, Damiano F. G. Fiorillo, and Ninetta Saviano, Direct detection of light dark matter from evaporating primordial black holes, Phys. Rev. D **105**, L021302 (2022).
[31] Wei Chao, Tong Li, and Jiajun Liao, Connecting primordial black hole to boosted sub-GeV dark matter through neutrino, arXiv:2108.05608.
[32] Kaustubh Agashe, Yanou Cui, Lina Necib, and Jesse Thaler, (In)direct detection of boosted dark matter, J. Cosmol. Astropart. Phys. 10 (2014) 062.
[33] Torsten Bringmann and Maxim Pospelov, Novel Direct Detection Constraints on Light Dark Matter, Phys. Rev. Lett. **122**, 171801 (2019).
[34] Christopher V. Cappiello, Kenny C. Y. Ng, and John F. Beacom, Reverse direct detection: Cosmic ray scattering with light dark matter, Phys. Rev. D **99**, 063004 (2019).
[35] Yohei Ema, Filippo Sala, and Ryosuke Sato, Light Dark Matter at Neutrino Experiments, Phys. Rev. Lett. **122**, 181802 (2019).
[36] Wen Yin, Highly-boosted dark matter and cutoff for cosmic-ray neutrinos through neutrino portal, EPJ Web Conf. **208**, 04003 (2019).
[37] James Alvey, Miguel Campos, Malcolm Fairbairn, and Tevong You, Detecting Light Dark Matter via Inelastic Cosmic Ray Collisions, Phys. Rev. Lett. **123**, 261802 (2019).
[38] James B. Dent, Bhaskar Dutta, Jayden L. Newstead, and Ian M. Shoemaker, Bounds on cosmic ray-boosted dark matter in simplified models and its corresponding neutrino-floor, Phys. Rev. D **101**, 116007 (2020).
[39] Joshua Berger, Yanou Cui, Mathew Graham, Lina Necib, Gianluca Petrillo, Dane Stocks, Yun-Tse Tsai, and Yue Zhao, Prospects for detecting boosted dark matter in DUNE through hadronic interactions, Phys. Rev. D **103**, 095012 (2021).
[40] Shao-Feng Ge, Jianglai Liu, Qiang Yuan, and Ning Zhou, Diurnal Effect of Sub-GeV Dark Matter Boosted by Cosmic Rays, Phys. Rev. Lett. **126**, 091804 (2021).
[41] Wonsub Cho, Ki-Young Choi, and Seong Moon Yoo, Searching for boosted dark matter mediated by a new gauge boson, Phys. Rev. D **102**, 095010 (2020).
[42] Chen Xia, Yan-Hao Xu, and Yu-Feng Zhou, Constraining light dark matter upscattered by ultrahigh-energy cosmic rays, Nucl. Phys. **B969**, 115470 (2021).
[43] Yohei Ema, Filippo Sala, and Ryosuke Sato, Neutrino experiments probe hadrophilic light dark matter, SciPost Phys. **10**, 072 (2021).
[44] Nicole F. Bell, James B. Dent, Bhaskar Dutta, Sumit Ghosh, Jason Kumar, Jayden L. Newstead, and Ian M. Shoemaker, Cosmic-ray upscattered inelastic dark matter, Phys. Rev. D **104**, 076020 (2021).
[45] Wenyu Wang, Wen-Na Yang, and Bin Zhu, The spin-dependent scattering of boosted dark matter, arXiv:2111.04000.
[46] Chen Xia, Yan-Hao Xu, and Yu-Feng Zhou, Production and attenuation of cosmic-ray boosted dark matter, J. Cosmol. Astropart. Phys. 02 (2022) 028.
[47] Yongsoo Jho, Jong-Chul Park, Seong Chan Park, and Po-Yan Tseng, Cosmic-neutrino-boosted dark matter (νBDM), arXiv:2101.11262.
[48] Anirban Das and Manibrata Sen, Boosted dark matter from diffuse supernova neutrinos, Phys. Rev. D **104**, 075029 (2021).

[49] Diptimoy Ghosh, Atanu Guha, and Divya Sachdeva, Exclusion limits on dark matter-neutrino scattering cross-section, arXiv:2110.00025.

[50] Jin-Wei Wang, Alessandro Granelli, and Piero Ullio, Direct detection constraints on Blazar-Boosted dark matter, arXiv:2111.13644.

[51] Carlos A. Argüelles, Alejandro Diaz, Ali Kheirandish, Andrés Olivares-Del-Campo, Ibrahim Safa, and Aaron C. Vincent, Dark matter annihilation to neutrinos, Rev. Mod. Phys. **93**, 035007 (2021).

[52] Gary Steigman, Basudeb Dasgupta, and John F. Beacom, Precise relic WIMP abundance and its impact on searches for dark matter annihilation, Phys. Rev. D **86**, 023506 (2012).

[53] Sergio Palomares-Ruiz and Silvia Pascoli, Testing MeV dark matter with neutrino detectors, Phys. Rev. D **77**, 025025 (2008).

[54] Nicole F. Bell, Matthew J. Dolan, and Sandra Robles, Searching for sub-GeV dark matter in the galactic centre using Hyper-Kamiokande, J. Cosmol. Astropart. Phys. 09 (2020) 019.

[55] Christopher V. Cappiello and John F. Beacom, Strong new limits on light dark matter from neutrino experiments, Phys. Rev. D **100**, 103011 (2019); **104**, 069901(E) (2021).

[56] Gordan Krnjaic and Samuel D. McDermott, Implications of BBN bounds for cosmic ray upscattered dark matter, Phys. Rev. D **101**, 123022 (2020).